Supporting information (SI)

"Cell fate decision mediated by p53 pulses"

Xiao-Peng Zhang, Feng Liu, Zhang Cheng, and Wei Wang

In this work, we aim at the p53 signaling network in untransformed mammalian cells, i.e., without genetic mutations in the involved factors of p53 response. We investigate the response of p53 signaling network to DNA damage in a population of 2000 cells. There are four modules in the model: a DNA repair module, an ataxia telangiectasia mutated (ATM) switch, the p53-Mdm2 oscillator and a cell fate decision module. Remarkably, we assume that p53 regulation of DNA repair is threshold-dependent, i.e., p53 promotes DNA repair when DNA damage is below a given threshold and otherwise suppresses DNA repair. In the following, we present the details of the model including equations and parameter values. The equations were solved numerically using a second-order Runge-Kutta algorithm with a time step $\Delta t = 0.01$, and the bifurcation diagrams are plotted using XPPAUT and Oscill 8.

Details of the Model

Stochastic Simulation of the Generation and Repair of DNA damage. Double-strand breaks (DSBs) are the predominant DNA lesions caused by ionizing radiation (IR). In mammalian cells, there are two major repair mechanisms for DSB repair: homologous recombination (HR) and nonhomologous end joining (NHEJ) [1, 2]. The NHEJ is the predominant pathway for DSB repair in mammalian cells, especially in G1 phase of the cell cycle [3]. There are two principal mechanisms for NHEJ: error-prone rejoining and precise ligation (error-free repair) [4]. The repair of IR-induced DNA damage is generally error-prone because IR destroys sequence information [4]. It has been proposed that p53 may control the fidelity of DSB repair by promoting precise repair but suppressing error-prone repair [1]. The fidelity of DSB repair reduces with increasing IR dose, and excessive DSBs may force normal NHEJ components to process DSBs aberrantly [5]. Therefore, we introduce the dose-dependent p53 regulation of DNA repair to the model, and assume that p53 promotes the DSB repair when the initial number of DSBs is below a threshold and otherwise suppresses the DSB repair. This threshold is set to 175, the mean number of DSBs produced at the radiation dose of $D_{\mathrm{IR}} = 5$ Gy.

Owing to stochasticity in the DNA repair process, we use the Monte Carlo method to simulate

the DNA repair dynamics. In the simulations, given the IR dose of y Gy, the initial number of DSBs in each cell is generated from a Poisson distribution with the mean of $35y$ [6], and the total number of DNA repair proteins is assumed to be 20 in each cell. We consider three states in the DSB repair process: intact DSB, DSB-protein complex (DSBC) and fixed DSB. For the sake of simplicity, the above three states are called state D, C and F, respectively. The numbers of DSBs in each state are represented by n_{D}, n_{C} and n_{F}, respectively. The schematic diagrams of DSB repair process are presented in Fig. S1. We use subscripts '1' and '2' to distinguish fast kinetics from slow kinetics [7]. The Monte Carlo algorithm for the repair dynamics is based on the transition probabilities between two neighboring states as follows:

$$\begin{aligned}
P_{D_1\to C_1} &= RP[k_{fb1} + k_{cross}(D_1 + D_2)]\Delta t \\
P_{D_2\to C_2} &= RP[k_{fb2} + k_{cross}(D_1 + D_2)]\Delta t \\
P_{C_1\to D_1} &= k_{rb1}\Delta t \\
P_{C_2\to D_2} &= k_{rb2}\Delta t \\
P_{C_1\to F_1} &= k_{fix1}\Delta t \\
P_{C_2\to F_2} &= k_{fix2}\Delta t.
\end{aligned} \tag{1}$$

In the above, all the ratios of the rates for the fast kinetics to those for the slow kinetic are chosen to be close to 10. It is also assumed that the binding of repair proteins to DSBs is much faster than other processes such as dissociation of repair proteins and the repair process. That is, the number of DSBCs is 20 when DSBs are more than repair proteins, while this number is equal to the number of DSBs when DSBs are fewer than repair proteins. We consider the p53 regulation of DNA repair, and the fixing rate of DNA repair should be p53-dependent. If $n_{\mathrm{D}} < 175$, the rates are described by

$$\begin{aligned}
k_{fix1} * (1 + \frac{[p53^*]}{1 + [p53^*]}), \\
k_{fix2} * (1 + \frac{[p53^*]}{1 + [p53^*]}).
\end{aligned} \tag{2}$$

If $n_{\mathrm{D}} \geq 175$, the rates are described by

$$\begin{aligned}
k_{fix1} * (1 - \frac{[p53^*]}{1 + [p53^*]}), \\
k_{fix2} * (1 - \frac{[p53^*]}{1 + [p53^*]}).
\end{aligned} \tag{3}$$

The Monte Carlo algorithm for the DBS repair dynamics at the IR dose of y Gy is presented in the following:

1. Generation of DSBs. Set t=0. The initial number of total DSBs $n_{\rm D}(0)$ is generated from a Poisson distribution with a mean value of 35y. The initial values for simple and complex DSB repair are taken as $n_{\rm D1}(0) = 0.7n_{\rm D}(0)$ and $n_{\rm D2}(0) = 0.3n_{\rm D}(0)$, respectively, while the numbers of DSBs in other states are set to zero, namely, $n_{\rm C1}(0) = n_{\rm C2}(0) = n_{\rm F1}(0) = n_{\rm F2}(0) = 0$. The total number of repair proteins $n_{\rm RP}$ is set to 20, and the number of free repair proteins is $n_{\rm RP}(0) = 20$.

2. Increasing time from t to $t = t + \triangle t$.

3. Update the states for each of the damages sites controlled by fast repair. For each damage locus i (with $1 \leq i \leq n_{\rm D1}(0)$), a random number r is generated from a uniform distribution between 0 and 1. If the damage at locus i is in state D, a transition to state C occurs if $0 \leq r < P_{D1\rightarrow C1}$, while it stays in state D if $P_{D1\rightarrow C1} \leq r \leq 1$. If the damage is in state C, a transition to state D occurs if $0 \leq r < P_{C1\rightarrow D1}$, or a transition to state F occurs if $P_{C1\rightarrow D1} \leq r < P_{C1\rightarrow D1} + P_{C1\rightarrow F1}$. If the damage is in state F, it always stays in state F (i.e., state F is absorbing). Set $n_{\rm RP} = n_{\rm RP} + 1$ if transition from state C to D or from state C to F occurs ; set $n_{\rm RP} = n_{\rm RP} - 1$ if transition from state D to C occurs; otherwise $n_{\rm RP}$ remains the same. After the last damage site has been updated, set the numbers of fast repaired breaks at time t in states D, C, and F to be $n_{\rm D1}$, $n_{\rm C1}$ and $n_{\rm F1}$, respectively.

4. Update the states for each of the damages sites controlled by slow repair. For each damage locus i (with $1 \leq i \leq n_{\rm D2}(0)$), a random number r is produced from a uniform distribution between 0 and 1. If the damage at locus i is in state D, a transition to state C occurs if $0 \leq r < P_{D2\rightarrow C2}$, while it stays in state D if $P_{D2\rightarrow C2} \leq r \leq 1$. If the damage is in state C, a transition to state D occurs if $0 \leq r \leq P_{C2\rightarrow D2}$, or a transition to state F occurs if $P_{C2\rightarrow D2} \leq r < P_{C2\rightarrow {\rm D}2} + P_{C2\rightarrow F2}$. If the damage is in state F, it always stays in state F (i.e., state F is absorbing). Set $n_{\rm RP} = n_{\rm RP} + 1$ if transition from state C to D or from state C to F occurs ; set $n_{\rm RP} = n_{\rm RP} - 1$ if transition from state D to C occurs; otherwise $n_{\rm RP}$ remains the same. After the last damage site has been updated, set the numbers of slow repaired breaks at time t in states D, C, and F to be $n_{\rm D2}$, $n_{\rm C2}$ and $n_{\rm F2}$, respectively.

5. Let $n_{\rm D}(t) = n_{\rm D1}(t) + n_{\rm D2}(t)$, $n_{\rm C}(t) = n_{\rm C1}(t) + n_{\rm C2}(t)$, and $n_{\rm F}(t) = n_{\rm F1}(t) + n_{\rm F2}(t)$.

6. Repeat steps 2-5 until all of the DSBs are effectively repaired, i.e., $n_{\rm D} \leq 2$.

Equations for the ATM Switch Module. Ataxia telangiectasia mutated (ATM) acts as a DSB detector and can be activated by DSBCs. The ATM switch module is composed of three

components: ATM dimer (ATM_2), inactive ATM monomer (ATM), and active ATM monomer (ATM^*) (Fig. S2). The dynamics of the ATM switch are characterized by ordinary differential equations (ODEs) as follows:

$$\begin{aligned} \frac{d[ATM_2]}{dt} &= k_{dim}[ATM]^2 - k_{undim}[ATM_2] && (4)\\ k_{1s} &= k_{1s0}[ATM^*]\frac{n_C}{n_C + j_{n_C}} \\ \frac{d[ATM^*]}{dt} &= k_{1s}\frac{[ATM]}{[ATM] + j_{1s}} - k_{2s}\frac{[ATM^*]}{[ATM^*] + j_{2s}} && (5)\\ [ATM] &= [ATM_{tot}] - 2[ATM_2] - [ATM^*] && (6) \end{aligned}$$

where $[ATM_2], [ATM]$ and $[ATM^*]$ are the concentrations of ATM dimers, inactive ATM monomers and active ATM monomers, respectively. In our model, the total concentration of ATM is assumed to be a constant, namely, $2[ATM_2] + [ATM] + [ATM^*] = [ATM_{tot}]$. The ATM monomers dimerize with a rate k_{dim}, and the ATM dimers disassociate with a rate k_{undim}. The rates of inactive ATM monomers activation and active monomers deactivation are k_{1s} and k_{2s}, respectively.

A positive feedback loop is significant for the activation of the ATM switch, i.e., the active ATM^* can promote the activation of inactive ATM through intermolecular autophosphorylation [8]. In addition, DSBCs can accelerate the activation of ATM^* [8], and k_{1s} is a function of the amounts of DSBC and ATM^*. Based on the positive feedback, the dynamics of ATM^* are characterized as a bistable switch, i.e., ATM^* level switches between two discrete 'on' and 'off' states, and this will send an on-off switching signal to the p53-Mdm2 oscillator.

Equations for the p53-Mdm2 Oscillator Module. The p53-Mdm2 oscillator can be initiated by the ATM switch. Two core proteins are involved in the p53-Mdm2 oscillator: p53 and Mdm2 (Fig. 2). Two forms of p53 in the nucleus are considered, inactive p53 and active $p53^*$, while the cytoplasmic p53 is not considered here. The Mdm2 in two compartments, $\mathrm{Mdm2_{nuc}}$ and $\mathrm{Mdm2_{cyt}}$, are involved, and they can shuttle between the nucleus and cytoplasm with rates k_i and k_o. Mdm2 acts as a ubiquitin ligase to target p53 for degradation by the proteasome. In the nucleus, inactive p53 is degraded rapidly by Mdm2 with a rate k_{d53}, while active $p53^*$ is degraded slowly with a rate k_{d53^*}. As a phosphorylation kinase, ATM^* induces the activation of p53 with a rate k_{ac}, and $p53^*$ can be deactivated with a basal rate k_{in}. For simplicity, we assume that both the degradation rate of Mdm2 and activation rate of p53 increase linearly with the ATM^* level.

Remarkably, two coupled positive and negative feedback loops are considered in the p53-Mdm2 oscillator module (Fig. 2). One is the negative feedback loop between p53* and $\mathrm{Mdm2_{nuc}}$: p53* promotes production of $\mathrm{Mdm2_{cyt}}$, which then enters the nucleus to targets p53 for degradation. The other is a positive feedback loop between p53* and $\mathrm{Mdm2_{cyt}}$: p53* induces *Mdm2* to synthesize $\mathrm{Mdm2_{cyt}}$, which promotes the translation of *p53* mRNA to produce inactive p53 [9]. It can be expected that robust and reliable p53 oscillations can be accomplished through a combination of negative and positive feedback loops rather than a single negative feedback loop with a time delay [10]. The corresponding dynamical equations for this module are presented as follows:

$$k_{d2} = k_{d21}(1 + [ATM^*]) \tag{7}$$

$$k_{ac} = k_{ac0}(1 + [ATM^*]) \tag{8}$$

$$k_{d53^*} = k_{d531} + k_{d532}G([Mdm2_{nuc}], \theta, J_{d53^*}/[p53^*, J_{d53^*}/[p53^*]) \tag{9}$$

$$k_{d53} = k_{d531} + k_{d532}G([Mdm2_{nuc}], \theta, J_{d53}/[p53], J_{d53}/[p53]), \tag{10}$$

where the Goldbeter-Koshland function, G, is defined as:

$$G(u, v, x, y) = \frac{2uy}{v - u + vx + uy + \sqrt{(v - u + vx + uy)^2 - 4(v - u)uy}}.$$

$$\frac{d[p53]}{dt} = k_{s531} + k_{s532}\frac{[Mdm2_{cyt}]^4}{j_{s53}^4 + [Mdm2_{cyt}]^4} + k_{in}[p53^*] - k_{ac}[p53] - k_{d53}[p53] \tag{11}$$

$$\frac{d[p53^*]}{dt} = k_{ac}[p53] - k_{in}[p53^*] - k_{d53^*}[p53^*] \tag{12}$$

$$\frac{d[Mdm2_{cyt}]}{dt} = k_{s21} + k_{s22}\frac{[p53^*]^4}{j_{s2}^4 + [p53^*]^4} - k_i[Mdm2_{cyt}] + k_o[Mdm2_{nuc}] - k_{d22}[Mdm2_{cyt}] \tag{13}$$

$$\frac{d[Mdm2_{nuc}]}{dt} = k_i[Mdm2_{cyt}] - k_o[Mdm2_{nuc}] - k_{d2}[Mdm2_{nuc}]. \tag{14}$$

Equations for the Cell Fate Decision Module. Many factors, such as stress signals, co-factors and post-translational modifications, can affect the stability and selectivity of p53 in target gene expression [11–13]. Especially, here two forms of active p53* are distinguished: p53 arrester and p53 killer (Fig. 3). p53 arrester is the primarily phosphorylated p53 on Ser15, while p53 killer refers to further phosphorylated p53, such as phosphorylated p53 on Ser46. p53 arrester regulates three target genes: *Wip1*, *p53DINP1* and *p21*, while p53 killer regulates two target genes: *p53DINP1* and *p53AIP1*. Two other apoptotic components are also included, namely, cytochrome c (CytoC) and Caspase 3 (Casp3) (Fig. 3).

The two forms of p53* perform different functions in cell fate decision. p53 arrester-induced p53DINP1 promotes phosphorylation of p53 on Ser46, i.e., formation of p53 killer, while Wip1 promotes reversion of p53 killer to p53 arrester. p53 arrester induces cell cycle arrest through activating CDK inhibitor p21, while p53 killer induces pro-apoptotic genes such as *p53AIP1*. Over-expression of *p53AIP1* can induce release of CytoC from mitochondria and activation of apoptosis executioner Casp3. Compared with the model by Zhang *et al.* [13], here two forms of p53 are considered by ignoring the intermediate one, and the complete process of apoptosis is characterized by including the ultimate activation of Casp3, which is the most reliable marker of apoptosis.

Here apoptosis is modeled as a bistable switch [14–16]. The 'life steady state' means no considerable caspases are activated, whereas 'death steady state' refers to almost full activation of caspases leading to apoptosis. In addition, we consider a positive feedback loop between CytoC and Casp3 (see Fig. 3). The release of CytoC leads to activation of Casp3, which in turn cleaves the inhibitors of p53AIP1 (such as Bcl-2 and Bcl-xL) to enhance release of CytoC [17, 18]. Therefore, a bistable switch can be constructed based on this positive feedback loop. Senescence due to permanent cell cycle arrest is not considered here. Moreover, although many inhibitors and enablers of apoptosis in the Bcl-2 family, like Bcl-2, Bcl-xL, Bax and Puma, are important to regulation of cell fate decision [19, 20], they are not considered here for the sake of simplicity. The detailed equations for this module are presented as follows:

$$\frac{d[p53\ killer]}{dt} = [p53DINP1]\frac{[p53\ arrester]}{j_{arrester}+[p53\ arrester]} - [Wip1]\frac{[p53\ killer]}{j_{killer}+[p53\ killer]} \quad (15)$$

$$[p53\ arrester] = [p53^*] - [p53\ killer] \quad (16)$$

$$\frac{d[Wip1]}{dt} = k_{sWip11} + k_{sWip12}\frac{[p53\ arrester]^3}{j_{sWip1}^3+[p53\ arrester]^3} - k_{dWip1}[Wip1] \quad (17)$$

$$\frac{d[p21]}{dt} = k_{sp211} + k_{sp212}\frac{[p53\ arrester]^3}{j_{sp21}^3+[p53\ arrester]^3} - k_{dp21}[p21] \quad (18)$$

$$\frac{d[p53DINP1]}{dt} = k_{sDINP11} + k_{sDINP12}\frac{[p53\ arrester]^3}{j_{sDINP11}^3+[p53\ arrester]^3} + k_{sDINP13}\frac{[p53\ killer]^3}{j_{sDINP12}^3+[p53\ killer]^3} - k_{dDINP1}[p53DINP1] \quad (19)$$

$$\frac{d[p53AIP1]}{dt} = k_{sAIP11} + k_{sAIP12}\frac{[p53\ killer]^3}{j_{sAIP1}^3+[p53\ killer]^3} - k_{dAIP1}[p53AIP1] \quad (20)$$

$$\frac{d[CytoC]}{dt} = k_{sCytoC}[p53AIP1]\frac{[Casp3]^4}{j_{Casp3}^4 + [Casp3]^4}[CytoC_{mito}] - k_{dCytoC}[CytoC] \quad (21)$$

$$\frac{d[Casp3]}{dt} = k_{sCasp31} + k_{sCasp32}\frac{[CytoC]^4}{j_{CytoC}^4 + [CytoC]^4} - k_{dCasp3}[Casp3] \quad (22)$$

$$[CytoC_{mito}] = [CytoC_{tot}] - [CytoC] \quad (23)$$

Details of the Results

The Connection Between Repair Time and Radiation Dose. Repair time is defined as the time taken for the number of DSBCs to reduce below two, i.e., $n_C \leq 2$. For a population of 2000 cells, the stochasticity in DNA repair is characterized in two aspects: the distribution of repair time and the mean repair time. Figure S3 shows the distribution of the repair time for the population at IR doses from 3 Gy to 7 Gy for the cases with and without p53 regulation of DNA repair. For the case without p53 regulation, the mean repair time increases monotonically with $D_{\rm IR}$, and the histograms shift rightward with increasing $D_{\rm IR}$ and are always unimodal (see the black lines).

Given the p53 regulation of DNA repair, the histograms are unimodal at low and high IR doses, while the histograms are bimodal around $D_{\rm IR}$=5 Gy. At low doses, p53 promotes the DNA repair with high fidelity, and thus the histograms for the cases with p53 regulation shift leftward (see the the first two histograms with red color in Fig.S3). At high doses, p53 suppresses the DNA repair, and the histograms shift rightward and become more widespread (see the last two histograms with red color in Fig. S3).

Interestingly, for the dose around $D_{\rm IR} = 5$ Gy, the histograms are bimodal (see the intermediate three histograms with red color in Fig. S3). These particular results originate from the threshold-dependent p53 regulation of DNA repair. p53 promotes the DNA repair when the initial number of DSBs is smaller than 175 but otherwise suppresses the DNA repair. That is, compared with the cases without p53 regulation, the repair time for some cells decreases due to the promotion of the repair and that for the others increases due to the suppression of the repair. As a result, the distribution of repair time is bimodal, composed of two small peaks.

Figure S4 displays the mean repair time for two cases. Clearly, the mean repair time for the case with p53 regulation is larger than that for the case without p53 regulation if $D_{IR} > 5$ Gy. This further identifies the dual role of p53 in DNA repair, i.e. p53 promotes DNA repair at low

IR doses but suppresses DNA repair at high doses.

The detailed dynamics of the ATM switch. As a detector of DSBs, ATM exhibits a switch-like behavior and plays a controlling role in setting a threshold level of DNA damage. Figure S5 displays the steady-state level of ATM* versus the number of DSBCs, $n_{\rm C}$. ATM activation starts with $n_{\rm C} = 5$, whereas ATM deactivation occurs when $n_{\rm C} = 2$, which ensures that DNA damage is effectively repaired (see the inset). Indeed, ATM is extremely sensitive to DNA damage; a $0.1 - 0.2$ Gy dose of IR can activate ATM. The simulation results are consistent with experimental observations, where 0.1-Gy IR can be detected by ATM and ATM activation becomes maximal at 0.5-Gy IR [8]. Figure S6 shows the time course of ATM* level for three individual cells at various IR doses. Upon IR, ATM is activated very rapidly, and ATM* level remains maximal over the first 800 min. Once $n_{\rm C}$ falls below a threshold (see Fig. S5), the ATM* level decays to zero much faster than $n_{\rm C}$. This sharp, step-like response of ATM* results from the positive feedback involved in ATM phosphorylation [8]. Clearly, the duration of active ATM prolongs with increased IR dose and is determined by the repair time. In addition, owing to stochasticity in DNA repair, cells exhibit considerable variability in the time courses of the ATM switch for IR with certain dose.

Parameter Dependence of P53 Oscillation. We change the values of parameters contained in this module by 20% around the control parameter set (the blue star) to check the robustness of p53 oscillation. The p53 level still exhibits periodic oscillations, and the variations in the period and amplitude of p53 pulses are constrained within 10% for most of the parameters (see Fig. S7). Especially, the period and amplitude of the oscillation is relatively sensitive to the synthesis and degradation rates of p53 and Mdm2. Our simulations also show that p53 oscillation will disappear if the basal induction rate of Mdm2 is increased 3-fold or the basal transcription rate of p53 is increased 4-fold (Fig. S8). This is consistent with the experimental observation that p53 oscillations were not observed in cells containing high-level Mdm2 as observed with a single nucleotide polymorphism in the *Mdm2* gene, which may contribute to tumorigenesis in those cells [21]. Therefore, too high level of p53 or Mdm2 fails to generate sustained oscillation, and only matched levels of p53 and Mdm2 generate the oscillation.

Damped Oscillation in Cell Population. It has been reported that p53 level exhibits damped oscillation at the population level upon IR [22]. Figure S9 shows the averaged p53 level over 2000 cells at IR doses of 1, 3 and 5 Gy. At the low dose of $D_{\rm IR}$ =1 Gy, the typical property

of the damped oscillation is observable, i.e., the p53 level exhibits decreasing amplitude in its second and third pulses. At the moderate dose of D_{IR}=3 Gy, the first two pulses have the same amplitude, but the amplitude drops since the third pulse. At D_{IR} = 5 Gy, the amplitude of pulses decays only after the fourth pulse. Here the damped oscillation of p53 level is consistent with the distribution of the pulse number in Fig. 7*D*. At D_{IR}=1 Gy, the first pulse of p53 level exists in almost all cells, while the second and third pulses only appear in some cells. Thus, the mean p53 level shows damped oscillation. When increasing D_{IR}, all the cells share the first two or three pulses, and thus the amplitude of p53 level decays after the first two or three pulses.

Regulation of the Apoptotic Switch by p53AIP1. The ultimate fate of cells is decided by the apoptotic switch, which is controlled by p53 pulses. As a target gene of p53, *p53AIP1* can be induced only by pulses of p53 killer, and this is crucial for the subsequent initiation of the apoptotic switch. Fig. S10 shows the bifurcation diagram of [Casp3] versus [p53AIP1]. The steady state of [Casp3] dose show the property typical of a bistable switch, i.e., a high level of p53AIP1 (about 0.7) turns on the switch with full activation of Casp3, and a rather low level of p53AIP1 (about 0.006) turns off the switch. According to our model, the basal level of p53AIP1 is about 0.08, which is much higher than the deactivated threshold (0.006). Thus, the apoptotic switch becomes irreversible after it is turned on. Our modeling is consistent with previous experimental observation that apoptosis is really irreversible after 'the point of no return'.

Integration of the levels of p53AIP1 and Casp3 over p53 pulses. In Fig. S11, two distinct cell fates are presented at the same radiation dose of D_{IR}=5 Gy. It is shown that the levels of p53AIP1 and p53 killer are gradually integrated over the pulses of p53 helper relying on the extent of DNA damage. If DNA damage is quickly repaired, the integration of p53AIP1 is not sufficient to drive the executioner of apoptosis, Casp3, to exceed the certain threshold (the left column). Thus, the cell can recover to normal growth after transient p53 pulses. However, when DNA damage is severe, the level of p53AIP1 accumulates to a sufficiently high level and oscillates there owing to sustained p53 pulses (the right column). As a result, Casp3 is irreversibly activated, and apoptosis ensues.

Annotations on the Model. For the sake of simplicity, we did not consider senescence due to permanent cell cycle arrest [23]. We omitted some other factors related to apoptosis, like Bcl-2, Apaf1, Bax and Puma *etc.* [24]. Although these factors are important to the regulation

of apoptosis under some conditions, there is no direct evidence that they are target genes of p53 killer. Moreover, another important transcription factor E2F1 is not explicitly included in our model since its role is to enhance the apoptosis cooperating with p53 [25]. Nevertheless, its influence is partially implicated in our model through tuning parameter values. In addition, we did not consider a variety of p53 cofactors such as ASSP1, ASSP2, HIPK2 and Hzf [26], which may be important to the promoter selectivity of p53. But our model can be easily extended to include these cofactors since it represents a general framework for cell fate decision by p53 pulses. Finally, note that the stochasticty is only involved in the DNA repair module, and intrinsic noise from gene expression in the other modules is not considered. Therefore, it is intriguing to investigate the effects of intrinsic noise in the p53 network on cell fate decision.

Note that permanent p53 oscillations can occur in the transformed MCF7 cells [27], which are deficient in DNA repair and inducing apoptosis [28–30]. Considering the effects of DNA repair, our model can explain the the presence of p53 permanent oscillations in the transformed cells. We propose that the number of p53 pulses can be used to distinguish cell survival from apoptosis. Thus, our proposal that cell fate can be determined by counting the number of p53 pulses represents a plausible mechanism. Moreover, p53 level can admit various behaviors, such as monostablity, oscillations and bistability at different parameter settings in our model. It is easy to modify parameter values to accommodate new experimental observations in our integrated model.

[1] Sengupta S, Harris CC (2005) p53: traffic cop at the crossroads of DNA repair and recombination. *Nat Rev Mol Cell Biol* 6:44-55.

[2] Gatz SA, Wiesmuller L (2006) p53 in recombination and repair. *Cell Death Differ* 13:1003-1016.

[3] Burma S, Chen BPC, Chen DJ (2006) Role of non-homologous end joining (NHEJ) in maintaining genomic integrity. *DNA Repair* 5:1042-1048.

[4] Dahm-Daphi J, *et al.* (2005) Nonhomologous end-joining of site-specific but not of radiation-induced DNA double-strand breaks is reduced in the presence of wild-type p53. *Oncogene* 24:1663-1672.

[5] Brady N, Gaymes TJ, Cheung M, Mufti GJ, Rassool FV (2003) Increased error-prone NHEJ activity in myeloid leukemias is associated with DNA damage at sites that recruit key nonhomologous end-joining proteins. *Cancer Res* 63:1798-1805.

[6] Ma L, *et al.* (2005) A plausible model for the digital response of p53 to DNA damage. *Proc Natl Acad Sci USA* 102:14266-14271.

[7] Stewart RD (2001) Two-lesion kinetic model of double-strand break rejoining and cell killing. *Radiat Res* 156:365-378.

[8] Bakkenist CJ, Kastan MB (2003) DNA damage activates ATM through intermolecular autophosphorylation and dimer dissociation. *Nature* 421:499-506.

[9] Yin Y, Stephen CW, Luciani MG, Fahraeus R (2002) p53 stability and activity is regulated by Mdm2-mediated induction of alternative p53 translation products. *Nat Cell Biol* 4:462-467

[10] Pomerening JR, Kim SY, Ferrell JE Jr (2005) Systems-Level Dissection of the Cell-Cycle Oscillator: Bypassing Positive Feedback Produces Damped Oscillations. *Cell* 122:565-578.

[11] Vousden KH, Lu X (2002) Live or let die: the cell's response to p53. *Nat Rev Cancer* 2:594-604.

[12] Oren M (2003) Decision making by p53: life, death and cancer. *Cell Death Differ* 10:431-442.

[13] Zhang T, Brazhnik P, Tyson JJ (2007) Exploring mechanisms of the DNA-damage response: p53 pulses and their possible relevance to apoptosis. Cell Cycle 6:85-94.

[14] Bagci EZ, Vodovotz Y, Billiar TR, Ermentrout GB, Bahar I (2006) Bistability in apoptosis: roles of P53AIP1, Bcl-2, and mitochondrial permeability transition pores. *Biophys J* 90:1546-1559.

[15] Eissing T, *el al.* (2004) Bistability analyses of a caspase activation model for receptor-induced apoptosis. *J Biol Chem* 279:36892-36897.

[16] Legewie S, Blüthgen N, Herzel H (2006) Mathematical Modeling identifies inhibitors of apoptosis as mediators of positive feedback and bistability. *PLoS Compt Biol* 2:e120.

[17] Kim Y-M, Kim T-H, Seol D-W, Talanian RV, Billiar TR (1998) Nitric oxide suppression of apoptosis occurs in association with an inhibition of Bcl-2 cleavage and cytochrome c release. *J Biol Chem* 273:31437-31441.

[18] Kirsch DG, et al. (1999) Caspase-3-dependent cleavage of Bcl-2 promotes release of cytochrome c. *J Biol Chem* 274:21155-21161.

[19] Adams JM, Cory S (2006) The Bcl-2 apoptotic switch in cancer development and therapy. *Oncogene* 26:1324-1337.

[20] Youle RJ, Strasser A (2008) The BCL-2 protein family: opposing activities that mediate cell death. *Nat Rev Mol Cell Biol* 9:47-59.

[21] Hu W, et al. (2007) A single nucleotide polymorphism in the Mdm2 gene disrupts the oscillation of p53 and Mdm2 levels in cells. *Cancer Res* 67:2757-2765.

[22] Lev Bar-Or R, *et al.* (2000) Generation of oscillations by the p53-Mdm2 feedback loop: A theoretical and experimental study. *Proc Natl Acad Sci USA* 97:11250-11255.

[23] Campisi J, d'Adda di Fagagna F (2007) Cellular senescence: when bad things happen to good cells. *Nat Rev Mol Cell Biol* 8(9):729-740.

[24] Cory S, Adams JM (2002) The Bcl2 family: regulators of the cellular life-or-death switch. *Nat Rev Cancer* 2:647-656.

[25] Iaquinta PJ, Lees JA (2007) Life and death decisions by the E2F transcription factors. *Curr Opin Cell Biol* 19:649-657.

[26] Murray-Zmijewski F, Slee, EA, Lu X (2008) A complex barcode underlies the heterogeneous response of p53 to stress. *Nat Rev Mol Cell Biol* 9:702-712.

[27] Geva-Zatorsky N, *et al.* (2006) Oscillations and variability in the p53 system. *Mol Syst Biol* 2:2006.0033

[28] Blanc C, *et al.* (2000) Caspase-3 is essential for procaspase-9 processing and cisplatin-induced apoptosis of MCF-7 breast cancer cells. *Cancer Res* 60:4386-4390.

[29] Tyson JJ (2006) Another turn for p53. *Mol Syst Biol* 2:2006.0032.

[30] Francisco DC, *et al.* (2008) Induction and processing of complex DNA damage in human breast cancer cells MCF-7 and nonmalignant MCF-10A cells. *Free Radic Biol Med* 44:558-569.

Figure legends

Fig. S1: Schematic illustration of the generation and repair of DSBs. (A) DSB repair dynamics are characterized as a three-state process: DSB, DSB-protein complex and fixed DSB, and p53 promotes the repair of slightly damaged cells but suppresses the repair of irreparably damaged cells. (B) The two-lesion kinetic model of DNA repair. The model contains two parallel repair pathways with distinct reaction rates corresponding to fast and slow repair. The fast and slow kinetics refer to repair of simple and complex DSBs, respectively. D, C and F represent intact DSB, DSBC, and fixed DSB, respectively. Subscripts '1' and '2' are used to distinguish fast kinetics from slow kinetics.

Fig. S2: Illustration of the ATM switch. ATM predominantly exists as a dimer in unstressed cells. After DNA damage, intermolecular autophosphorylation occurs, and ATM dimers dissociate into active monomers. Here active ATM monomers can promote the formation of themselves, and the process is stimulated by DSBCs.

Fig. S3: Histogram of repair time for 2000 cells. The cell count versus the repair time is plotted for for the case with and without p53 regulation (red and black lines, respectively) at IR doses of 3, 4, 4.5, 5, 5.5, 6 and 7 Gy (from top to bottom).

Fig. S4: Mean repair time vs D_{IR} for the case with p53 regulation (red line) and without p53 regulation (black line). The mean repair time is obtained by averaging over 2000 individual cells.

Fig. S5: Bifurcation diagram of ATM* level vs n_{c}. Based on the positive feedback loop in the activation of ATM through intermolecular phosphorylation stimulated by DSBCs, ATM is modeled as a bistable switch. The switch is turned on with n_{C}=5, while it is turned off with n_{C}=2 (see the inset).

Fig. S6: Time courses of ATM* level for three individual cells at D_{IR}=4, 5, 6 Gy. On average, the duration of the switch in the 'ON' state prolongs with increasing D_{IR}. For certain D_{IR}, the duration displays considerable variability among three individual cells. The dotted lines indicates the threshold time for cell fate decision.

Fig. S7: Parameter sensitivity of the p53 oscillation. We show the dependence of the period and amplitude of p53 pulse on the parameter fluctuation. Here we change the values of parameters contained in this module by 20% around the control parameter set to check the robustness of p53 oscillation.

Fig. S8: Disappearance of p53 oscillation by increasing the basel transcription rate of p53 (k_{s531}) 4-fold, and that of Mdm2 (k_{s21}) 3-fold, respectively, at D_{IR}= 5 Gy. (A) p53 dynamics in three individual cells with $k_{s531} = 0.075$; (B) p53 dynamics in three individual cells with $k_{s21} = 0.016$.

Fig. S9: Damped oscillation of the mean p53 level averaged over a population of 2000 cells at D_{IR}= 1, 3 and 5 Gy. At low IR doses, typical properties of damped oscillation are observable. At D_{IR}= 3 and 5 Gy, the amplitudes decay in the last three pulses, while the first several pulses keep the same amplitude.

Fig. S10: Bifurcation diagram of Caspase 3 vs p53AIP1. The apoptotic switch is initiated by p53AIP1 with a level above a threshold (see the blue arrow), while it is turned off by p53AIP1 with a level close to zero (0.006). The resting state of p53AIP1 is about 0.08 (see the red arrow). That is, once the switch is turned on, it can remain in the 'ON' state even after the level of p53AIP1 drops to the resting state. Thus, the apoptotic switch becomes irreversible.

Fig. S11 : Time courses of the levels of p53 helper, p53 killer, p53AIP1 and Casp3 in two individual cells at D_{IR}=5 Gy. Two cells show distinct cell fates due to variability in the initial number of DSBs and the repair dynamics.

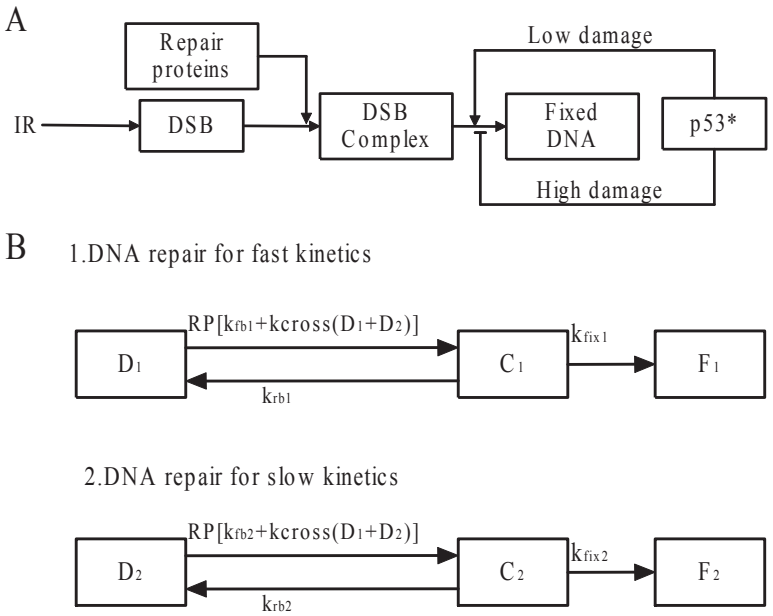
A
Repair proteins
IR
DSB
DSB Complex
Fixed DNA
p53*
Low damage
High damage
B
1.DNA repair for fast kinetics
RP[kfb1+kcross(D1+D2)]
D1
C1
F1
krb1
kfix1
2.DNA repair for slow kinetics
RP[kfb2+kcross(D1+D2)]
D2
C2
F2
krb2
kfix2

Fig.S1

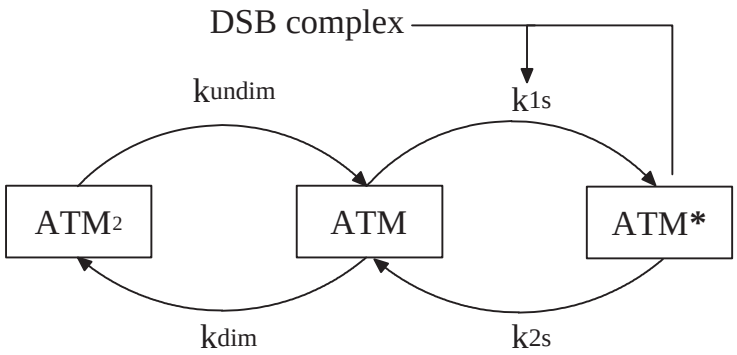
DSB complex
kundim
k1s
ATM2
ATM
ATM*
kdim
k2s

Fig.S2

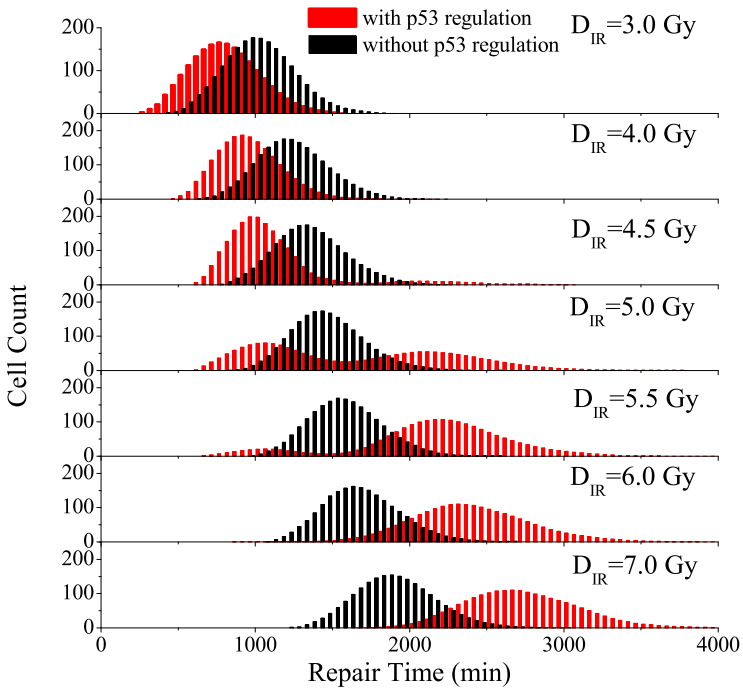
with p53 regulation
without p53 regulation
D_IR=3.0 Gy
D_IR=4.0 Gy
D_IR=4.5 Gy
D_IR=5.0 Gy
D_IR=5.5 Gy
D_IR=6.0 Gy
D_IR=7.0 Gy
Cell Count
Repair Time (min)
0
100
200
1000
2000
3000
4000

Fig.S3

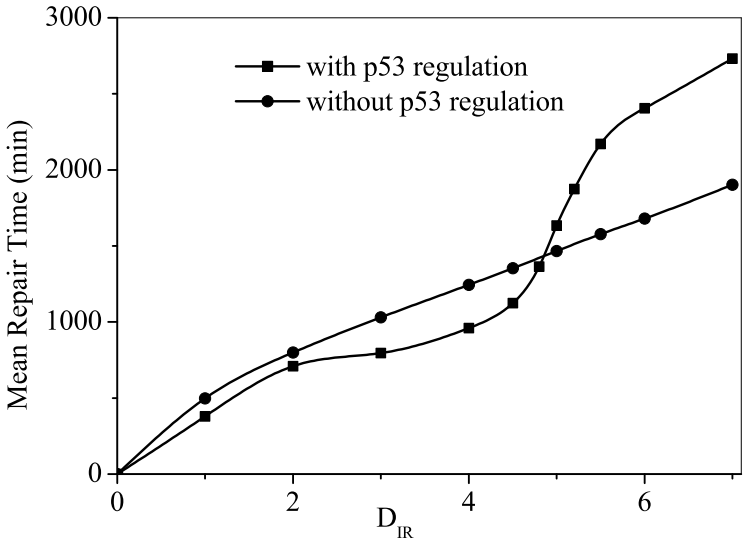
with p53 regulation
without p53 regulation
Mean Repair Time (min)
D_IR
0
1000
2000
3000
2
4
6

Fig.S4

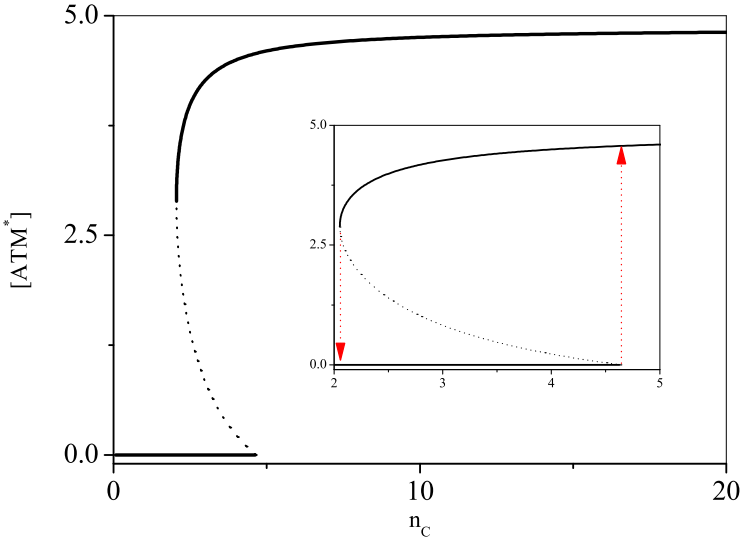
5.0
2.5
0.0
[ATM*]
0
10
20
n_C
5.0
2.5
0.0
2
3
4
5

Fig.S5

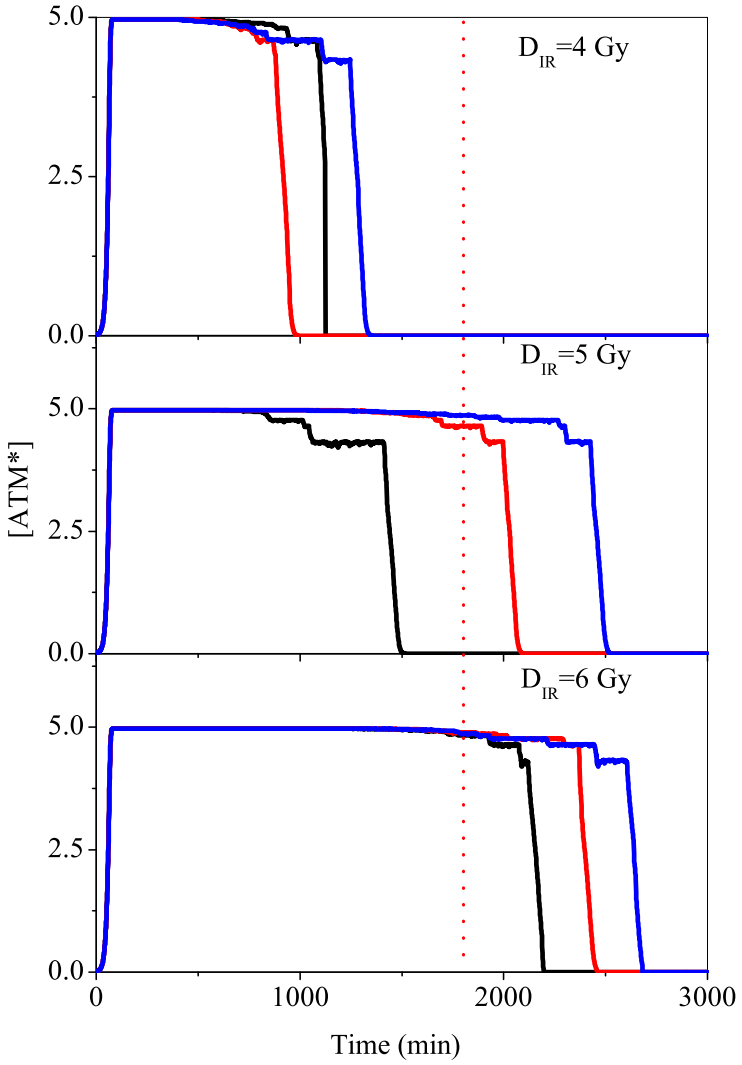
D_IR=4 Gy
D_IR=5 Gy
D_IR=6 Gy
[ATM*]
5.0
2.5
0.0
0
1000
2000
3000
Time (min)

Fig.S6

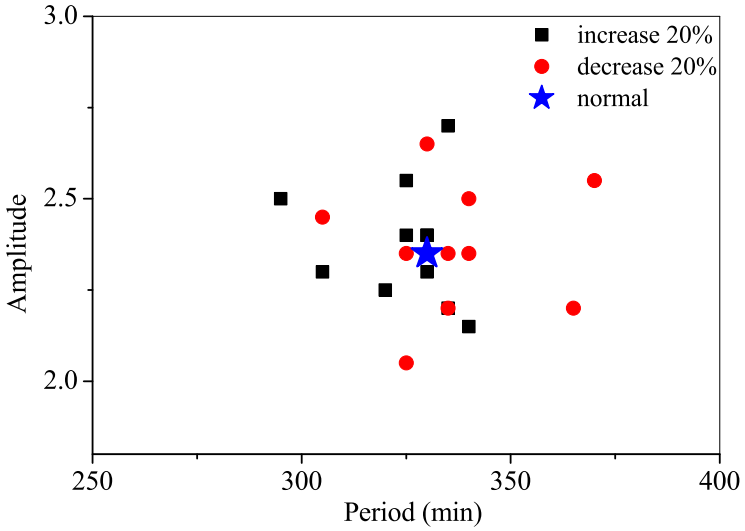
3.0
2.5
2.0
Amplitude
250
300
350
400
Period (min)
increase 20%
decrease 20%
normal

Fig.S7

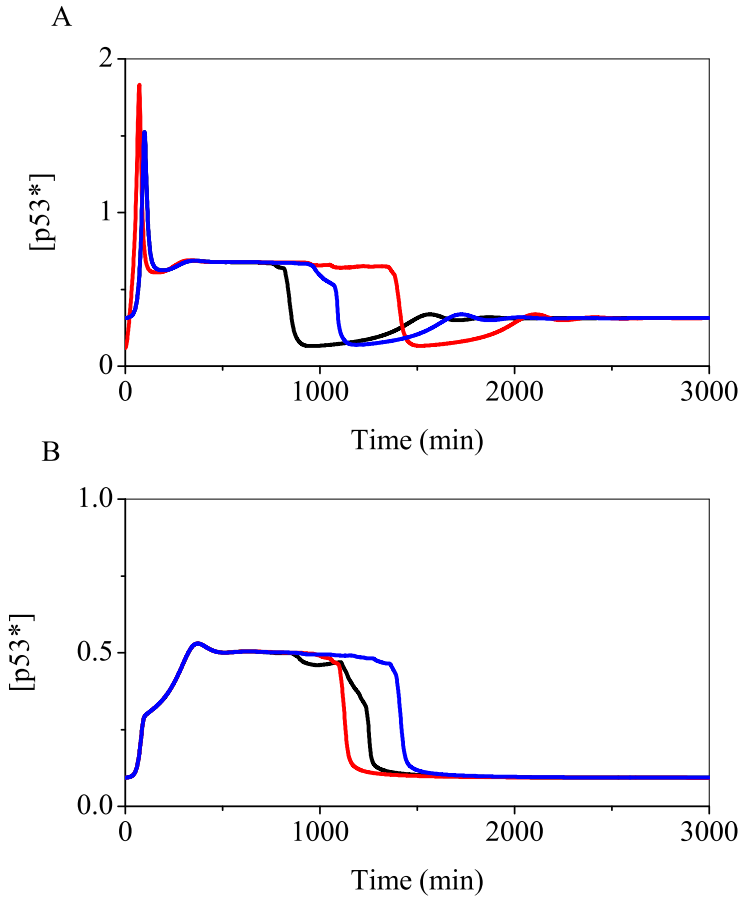
A
2
1
0
[p53*]
0
1000
2000
3000
Time (min)
B
1.0
0.5
0.0
[p53*]
0
1000
2000
3000
Time (min)

Fig.S8

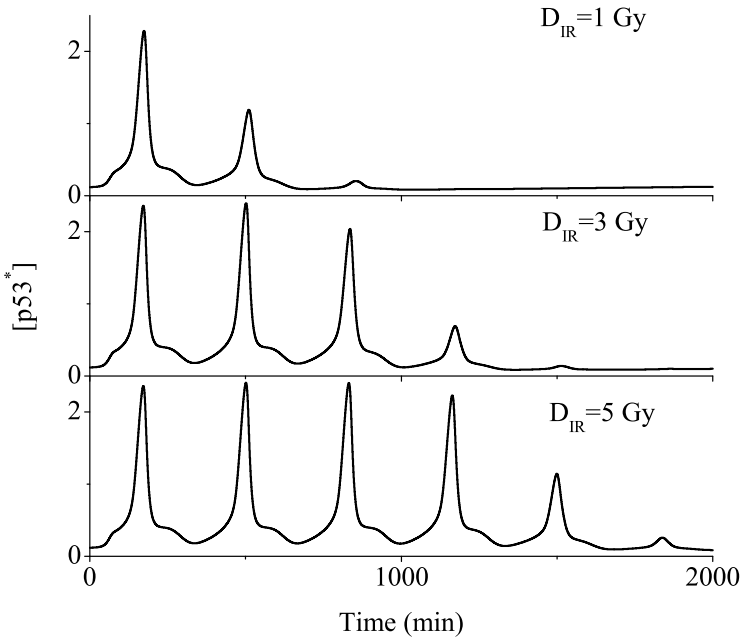

Fig.S9

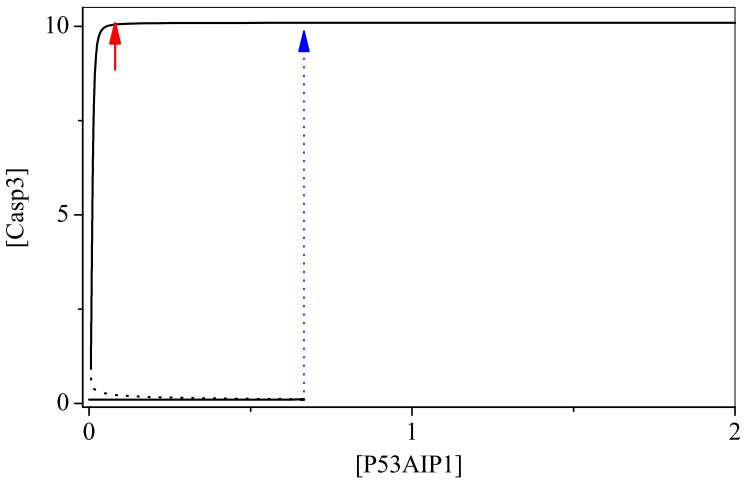

Fig.S10

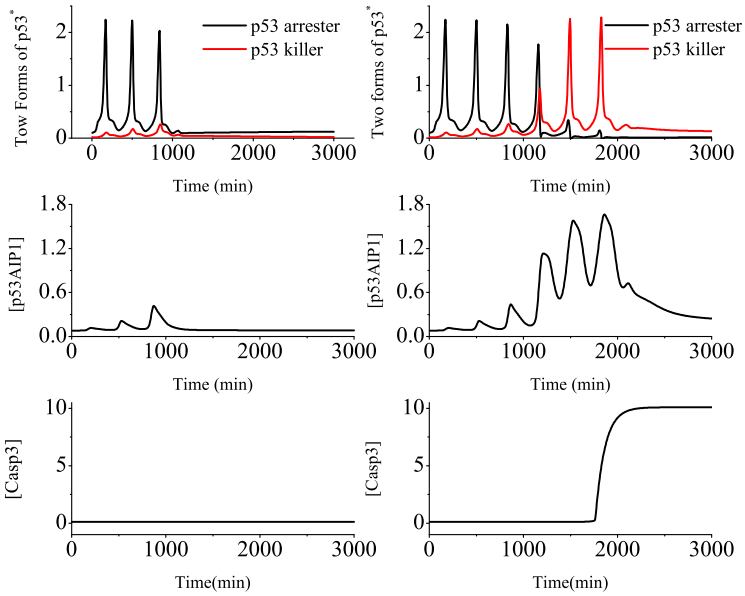
Tow Forms of p53*
p53 arrester
p53 killer
Time (min)
Two forms of p53*
p53 arrester
p53 killer
Time (min)
[p53AIP1]
Time (min)
[p53AIP1]
Time (min)
[Casp3]
Time(min)
[Casp3]
Time(min)

Fig.S11

TABLE I: Parameters for the whole model

Rate Constant	Description	Value
RPT	Number of repair proteins	20
k_{fb1}	Association rate of repair proteins in fast kinetics	2
k_{fb2}	Association rate of repair proteins in slow kinetics	0.2
k_{rb1}	Dissociation rate of repair proteins in fast kinetics	0.5
k_{rb2}	Dissociation rate of repair proteins in slow kinetics	0.05
k_{fix1}	DSB ligation rate in fast kinetics	0.03
k_{fix2}	DSB ligation rate in slow kinetics	0.003
k_{cross}	DSB binary mismatch rate	0.001
k_{dim}	ATM dimerization rate	5
k_{undim}	ATM undimerization rate	1
k_{1s0}	Basal activation rate of ATM	1.5
k_{2s}	ATM inactivation rate	0.8
j_{1s}	Michaelis constant of ATM activation	1
j_{2s}	Michaelis constant of ATM^* inactivation	2.5
j_{nC}	Threshold number of DSBC for ATM activation	4
ATM_{tot}	the total concentration of all forms of ATM	5
k_{s531}	Basal induction rate of p53	0.0016
k_{s532}	Mdm2-dependent production rate of p53	0.08
k_{d531}	Basal degradation rate of p53	0.0016
k_{d532}	Mdm2-dependent degradation rate of p53	0.08
θ	Threshold concentration for Mdm2-dependent p53 degradation	0.83
J_{d53^*}	Threshold concentration of p53* for Mdm2-dependent degradation	0.1
J_{d53}	Threshold concentration of p53 for Mdm2-dependent degradation	0.01
k_{d21}	Basal degradation rate of $Mdm2_{nuc}$	0.0013
k_{d22}	Degradation rate of $Mdm2_{cyt}$	0.0013
k_{s21}	Basal induction rate of $Mdm2_{cyt}$	0.004
k_{s22}	p53-dependent production rate of Mdm2	0.11
j_{s53}	threshold concentration of Mdm2-dependent p53 production	0.45
j_{s2}	Michaelis constant of p53-dependent Mdm2 production	0.92
k_i	Nuclear import rate of $Mdm2_{cyt}$	0.01
k_o	Nuclear export rate of $Mdm2_{nuc}$	0.0013
k_{ac}	Activation rate of $p53$	0.026
k_{in}	Inactivation rate of $p53^*$	0.0013

k_{sWip11}	Basal induction rate of $Wip1$	0.00054
k_{sWip12}	$p53$ *arrester* dependent production rate of $Wip1$	0.04
j_{sWip1}	Michaelis constant of $p53$ *arrester* dependent $Wip1$ production	1.8
k_{dWip1}	Degradation rate of $Wip1$	0.001
k_{sp211}	Basal induction rate of $p21$	0.0001
k_{sp212}	$p53$ *arrester* dependent production rate of $p21$	0.135
j_{sp21}	Michaelis constant of $p53$ *arrester* dependent $p21$ production	2
k_{dp211}	Degradation rate of $p21$	0.0054
$k_{sDINP11}$	Basal induction rate of $p53DINP1$	0.000054
$k_{sDINP12}$	$p53$ *arrester* dependent production rate of $p53DINP1$	0.0027
$k_{sDINP13}$	$p53$ *killer* dependent production rate of $p53DINP1$	0.135
$j_{sDINP11}$	Michaelis constant of $p53$ *arrester* dependent $p53DINP1$ production	0.4
j_{DINP12}	Michaelis constant of $p53$ *killer* dependent $p53DINP1$ production	0.5
k_{dDINP1}	Degradation rate of $p53DINP1$	0.00135
k_{sAIP11}	Basal induction rate of $p53AIP1$	0.0011
k_{sAIP12}	$p53$ *killer* dependent production rate of $p53AIP1$	0.027
j_{sAIP1}	Michaelis constant of $p53$ *killer* dependent $p53AIP1$ production	0.3
k_{dAIP1}	Degradation rate of $p53AIP1$	0.0135
k_{sCytoC}	P53AIP1 dependent cytochrome c activation rate	0.1
k_{dCytoC}	Inactivation rate of cytochrome c	0.005
$k_{sCasp31}$	Basal induction rate of Caspase 3	0.001
$k_{sCasp32}$	cytochrome c dependent production rate of Caspase 3	0.1
k_{dCasp3}	Degradation rate of Caspase 3	0.01
j_{CytoC}	Michaelis constant of Caspase 3 dependent cytochrome c production	0.3
j_{Casp3}	Michaelis constant of cytochrome c dependent Caspase 3 production	0.3
$CytoCtot$	Total concentration of cytochrome c	3